

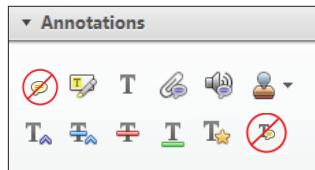
Page Proof Instructions and Queries

Journal Title: PIH
Article Number: 606150

Greetings, and thank you for publishing with SAGE. We have prepared this page proof for your review. Please respond to each of the below queries by digitally marking this PDF using Adobe Reader.

Click “Comment” in the upper right corner of Adobe Reader to access the mark-up tools as follows:

For textual edits, please use the “Annotations” tools.
 Please refrain from using the two tools crossed out below, as data loss can occur when using these tools.



For formatting requests, questions, or other complicated changes, please insert a comment using “Drawing Markups.”



Detailed annotation guidelines can be viewed at: <http://www.sagepub.com/repository/binaries/pdfs/AnnotationGuidelines.pdf>
 Adobe Reader can be downloaded (free) at: <http://www.adobe.com/products/reader.html>.

Sl. No.	Query
1	GQ: Please confirm that all author information, including names, affiliations, sequence, and contact details, is correct.
2	GQ: Please review the entire document for typographical errors, mathematical errors, and any other necessary corrections; check headings, tables, and figures.
3	GQ: Please ensure that you have obtained and enclosed all necessary permissions for the reproduction of artworks (e.g. illustrations, photographs, charts, maps, other visual material, etc.) not owned by yourself. please refer to your publishing agreement for further information.
4	GQ: Please note that this proof represents your final opportunity to review your article prior to publication, so please do send all of your changes now.
5	GQ: Please confirm that the acknowledgement, funding and conflict of interest statements are accurate.
6	AQ: Please check whether ‘1.2 × body weight’ is correct as set in the sentence ‘They also simulate ...’.
7	AQ: Please check whether ‘three-second pause’ is correct as set in the sentence ‘For each cycle, the actuator ...’.
8	AQ: Please check whether the edits made to the caption of Figure 10 are correct.
9	AQ: Please provide the significance of bold value in Table 2.
10	AQ: Ref. 24 is not cited in text. Please indicate where a citation should appear or delete the reference.

- GQ: Please confirm that all author information, including names, affiliations, sequence, and contact details, is correct.
- GQ: Please review the entire document for typographical errors, mathematical errors, and any other necessary corrections; check headings, tables, and figures.
- GQ: Please ensure that you have obtained and enclosed all necessary permissions for the reproduction of artworks (e.g. illustrations, photographs, charts, maps, other visual material, etc.) not owned by yourself. please refer to your publishing agreement for further information.
- GQ: Please note that this proof represents your final opportunity to review your article prior to publication, so please do send all of your changes now.
- GQ: Please confirm that the acknowledgement, funding and conflict of interest statements are accurate.
- 1 AQ: Please check whether ‘1.2 × body weight’ is correct as set in the sentence ‘They also simulate ...’.
- 2 AQ: Please check whether ‘three-second pause’ is correct as set in the sentence ‘For each cycle, the actuator ...’.
- 3 AQ: Please check whether the edits made to the caption of Figure 10 are correct.
- 4 AQ: Please provide the significance of bold value in Table 2.
- 5 AQ: Ref. 24 is not cited in text. Please indicate where a citation should appear or delete the reference.

The design and validation of a magnetic resonance imaging-compatible device for obtaining mechanical properties of plantar soft tissue via gated acquisition

Evan D Williams^{1,2}, Michael J Stebbins^{1,2}, Peter R Cavanagh^{2,3},
 David R Haynor⁴, Baocheng Chu⁴, Michael J Fassbind¹, Vara Isvilanonda^{1,2}
 and William R Ledoux^{1,2,3}

Abstract

Changes in the mechanical properties of the plantar soft tissue in people with diabetes may contribute to the formation of plantar ulcers. Such ulcers have been shown to be in the causal pathway for lower extremity amputation. The hydraulic plantar soft tissue reducer was designed to measure in vivo, rate-dependent plantar soft tissue compressive force and three-dimensional deformations to help understand, predict, and prevent ulcer formation. These patient-specific values can then be used in an inverse finite element analysis to determine tissue moduli, and subsequently used in a foot model to show regions of high stress under a wide variety of loading conditions. The hydraulic plantar soft tissue reducer uses an actuator to drive a magnetic resonance imaging-compatible hydraulic loading platform. Pressure and actuator position were synchronized with gated magnetic resonance imaging acquisition. Achievable loading rates were slower than those found in normal walking because of a water-hammer effect (pressure wave ringing) in the hydraulic system when the actuator direction was changed rapidly. The subsequent verification tests were, therefore, performed at 0.2 Hz. The unloaded displacement accuracy of the system was within 0.31%. Compliance, presumably in the system's plastic components, caused a displacement loss of 5.7 mm during a 20-mm actuator test at 1354 N. This was accounted for with a target to actual calibration curve. The positional accuracy of the hydraulic plantar soft tissue reducer during loaded displacement verification tests from 3 to 9 mm against a silicone backstop was 95.9% with a precision of 98.7%. The hydraulic plantar soft tissue reducer generated minimal artifact in the magnetic resonance imaging scanner. Careful analysis of the synchronization of the hydraulic plantar soft tissue reducer and the magnetic resonance imaging scanner was performed. With some limitations, the hydraulic plantar soft tissue reducer provided key functionality in measuring dynamic, patient-specific plantar soft tissue mechanical properties.

Keywords

Heel pad, diabetes, magnetic resonance imaging-compatible, mechanical properties

Date received: 16 April 2015; accepted: 19 August 2015

Introduction

Diabetes mellitus (DM) is a major public health problem in the United States with 9.3% of the population having the disease in 2014. A diagnosis of DM is present in 60% of patients undergoing non-traumatic lower limb amputations.¹ The disease has been shown to increase the modulus of plantar soft tissue in cadaveric samples,² and this affects the ability of the foot to absorb and distribute energy from loading. As a result, peak stresses in plantar tissue near bony prominences

¹RR&D Center of Excellence for Limb Loss Prevention and Prosthetic Engineering, VA Puget Sound Health Care System, Seattle, WA, USA

²Department of Mechanical Engineering, University of Washington, Seattle, WA, USA

³Department of Orthopaedics & Sports Medicine, University of Washington, Seattle, WA, USA

⁴Department of Radiology, University of Washington, Seattle, WA, USA

Corresponding author:

William R Ledoux, RR&D Center of Excellence for Limb Loss Prevention and Prosthetic Engineering, VA Puget Sound Health Care System, ms 151, VA Puget Sound, 1660 S. Columbian Way, Seattle, WA 98108, USA.
 Email: wrlledoux@uw.edu

can increase fourfold or more³ and are thought to be the location of initial ulcer formation.^{3,4} There is a need to improve current methods for predicting internal stress due to increases in plantar tissue stiffness. This can be accomplished by advancing the technology for measuring patient-specific soft tissue material properties. When combined with finite element analysis (FEA), this will allow improved understanding of foot mechanics and the development of patient-specific treatment options.

Ultrasound and fluoroscopic imaging have been previously used in plantar tissue analyses.^{5–7} Cavanagh⁶ mounted an ultrasound probe flush with an acrylic plate that measured skin-to-metatarsal head displacements upon foot contact. These measurements were one-dimensional (1D) and load data were collected in a subsequent test using separate equipment. Erdemir et al.⁷ utilized an ultrasound indenter in conjunction with dynamic loading and inverse FEA to develop hyperelastic material properties of the plantar fat pad. The device was capable of controlling the loading rate and recording patient-specific thickness, but the study approximated the fat pad as axisymmetric with idealized boundary conditions and considered only a single dimension. Gefen et al.⁵ used fluoroscopy and a force plate for simultaneous load and deformation collection, but this work was also limited to a single dimension and exposed the patient to ionizing radiation. Although the above studies are the foundation for subsequent work, it is difficult to extrapolate their results to the generation of three-dimensional (3D) patient-specific FEA models.

Progressing beyond ultrasound and fluoroscopy, plantar tissue properties can also be determined by magnetic resonance imaging (MRI), in conjunction with various non-metallic loading instruments. Petre et al.⁸ developed a device that applied compressive loads to feet by holding hydraulic pressures for 3.5 min static MRI scans. The resulting material property estimates could potentially be improved by including strain rate-dependent effects, which might be significant.² Gefen et al.⁹ employed an MRI-compatible spherical indentation device to measure load versus displacement of the plantar soft tissue between metatarsal heads. In addition to also being a static test, the less than 2 N loads were much smaller than would occur during normal loading. In addition, the skin, fat, and other subcutaneous tissues were lumped into one generic soft tissue composite. Another indenter study by Brown et al.¹⁰ addressed the viscoelastic dependency of tissue with another MRI-compatible piezoelectric device that accounted for strain and strain rate. The system has been used with tissue samples, but it is not understood if this technique can be applied to living subjects. Weaver et al.¹¹ performed dynamic magnetic resonance (MR) elastography and determined that shear moduli differed with applied load. However, subjects voluntarily controlled the force and only two loading points were studied.

The purpose of this study was to develop a plantar soft tissue testing apparatus that allows for dynamic plantar loading at the hindfoot or forefoot in living subjects at physiologic force during gait while simultaneously capturing 3D soft tissue deformation. Subsequent FEA models will incorporate patient-specific anatomy and differentiation between soft tissue types. Hereafter, we report on the development and validation of the hydraulic plantar soft tissue reducer (HyPSTR), which loads the foot with a hydraulic system and records 3D tissue deformations with gated MRI.

Methods

System design

The HyPSTR was designed to acquire gated MR images from multiple phases of internal tissue deformation during displacement-controlled cyclic loading of the plantar aspect of the foot. In total, 16 phases were used in the experiments reported here, a single-acting, master/slave hydraulic loading device produced triangle or sine shaped displacement curves of 10 mm maximum amplitude at theoretical loading rates up to 6 Hz and a maximum load of 1500 N. These parameters exceed the largest displacement necessary to approximate strain under body weight loading of the maximum plantar fat pad thickness expected.^{12–18} They also simulate the frequency content of gait¹⁹ and allow for 1.2 × body weight forces for most people.

All equipment in the MRI room was non-metallic, except for a few small, non-replaceable, but well secured, hardware items. Equipment in the control room, including all actuation, control, and data acquisition components did not have metallic restrictions (Figure 1). Electrical components were designed to minimize electromagnetic interference from the MR by utilizing twisted-pair shielded wiring, metal enclosures, and analog filtered signal lines. The displacement control system was built from a stepper motor-driven linear actuator (The Bug; Ultra Motion, Cutchogue, NY) and a stand-alone stepper driver (ST5-Si; Applied Motion Products Inc., Watsonville, CA).

A custom-designed, single-acting, aluminum master piston/cylinder was attached to the actuator. The slave piston/cylinder was a similarly designed, single-acting hydraulic system with equal bore diameter, but made of non-ferrous acetal plastic. A polycarbonate loading platen, threaded onto the end of the slave piston shaft, applied load to the plantar surface of the foot. The master and slave cylinders were connected via 9 m of 9.65 mm internal diameter, vacuum-rated nylon tubing that could withstand more than the 20-kPa negative pressure during the hydraulic retraction stage. Water was chosen as the hydraulic fluid because of its relative safety, and ease of handling compared to various oils and gels. A recirculation pump moved the water through a hydronic air eliminator (VJR075TM; Spirotherm, Glendale Heights, IL) to lower the

AQ1

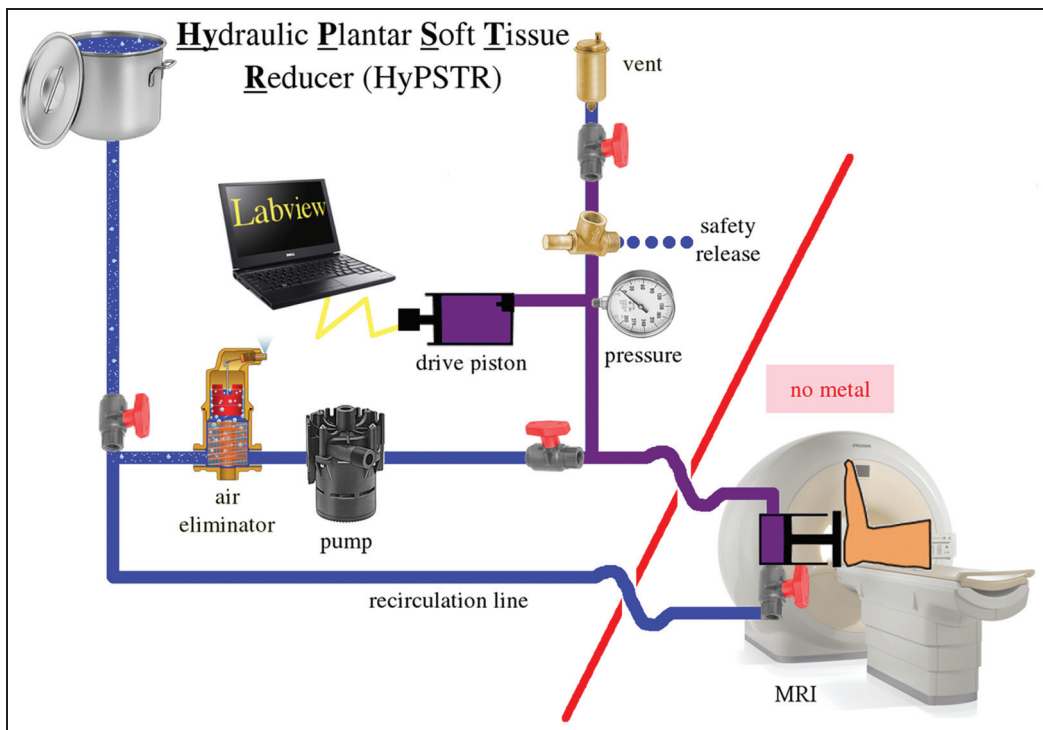


Figure 1. Instrument schematic showing fill and recirculation lines in blue and high-pressure hydraulic lines in purple. Valves were closed to isolate the purple lines prior to testing. The red line separates the MRI control and imaging rooms.

dissolved gas below 50% to prevent entrained air bubbles from forming during system operation.

Manufacturer-provided software (Q-Programmer) controlled the stepper driver. Custom LabVIEW software acquired and logged data, sent the displacement-synchronized trigger signal to the MR control center, and monitored the solenoid hydraulic safety valve. The software ran on a laptop computer (Intel Pentium M, 1.6 GHz, 2.0 GB RAM), which hosted an external data acquisition board (USB-6212, 400 kS/s, 16 bits; National Instruments, Austin, TX). All signals were acquired at 2500 Hz to allow for digital post-processing. A rotary encoder affixed to the stepper motor (The Bug; Ultra Motion, Cutchogue, NY) measured the position and velocity of the linear actuator. A pressure transducer (PX209-200; Omega Engineering, Stamford, CT) installed in the hydraulic system monitored the load applied to the foot. System pressure measurements during each of the 16 phases were translated to applied force values with a calibration curve that was generated using the HyPSTR to compress a piece of silicon in series with a 500-N load cell (MC3A-500; AMTI, Watertown, MA).

The test subject lay supine in an apparatus that supported the slave cylinder and loading platen and restrained the subject's foot, leg, and torso in order to minimize movement in the imaged volume that was not due to foot tissue compression (Figure 2). The lower leg was secured with a hindfoot ankle-foot orthosis (American Artificial Limb, Seattle, WA) made from carbon fiber, leather, fiberglass, and Pe-Lite foam

secured. A cutout in the sole allowed loading access to the heel (Figure 3). This could be swapped for a second, forefoot ankle-foot orthosis that provided a back-stop for the foot dorsum during forefoot testing. The slave cylinder could be adjusted in the anterior/posterior direction to align the loading platen with the center of the hindfoot or forefoot, and in the medial/lateral direction to adjust for left or right feet. To further minimize motion, the subject's torso was held in place with adjustable straps over the shoulders and around the waist connected to a backboard that is integrated into the apparatus. All frame components and fasteners were polycarbonate, acetal plastic, nylon, fiberglass, polypropylene, or polyethylene (i.e. non-metallic).

In an MRI, moving tissue can be imaged with cardiac gating, where several short image phase acquisitions are triggered by the subject's heartbeat (1 cycle). Only objects with a periodic or quasi-periodic motion can be imaged in this manner,²⁰ which, in this study, referred to a foot being moved by the loading platen. Instead of using a heartbeat, phase synchronization was accomplished with a 2-ms peripheral pulse unit (PPU) signal sent to the MRI scanner from a custom LabVIEW VI via a serial-to-fiber-optic signal converter (Versalink; Electro Standards Laboratory, Cranston, RI). A pulse was sent upon initial movement of the actuator from its zero-position and was then repeated at the start of each displacement cycle until scan completion. The 3.0-T Philips Achieva MRI Control and Data Acquisition System (Amsterdam) received this PPU and initiated the phase recording protocol in

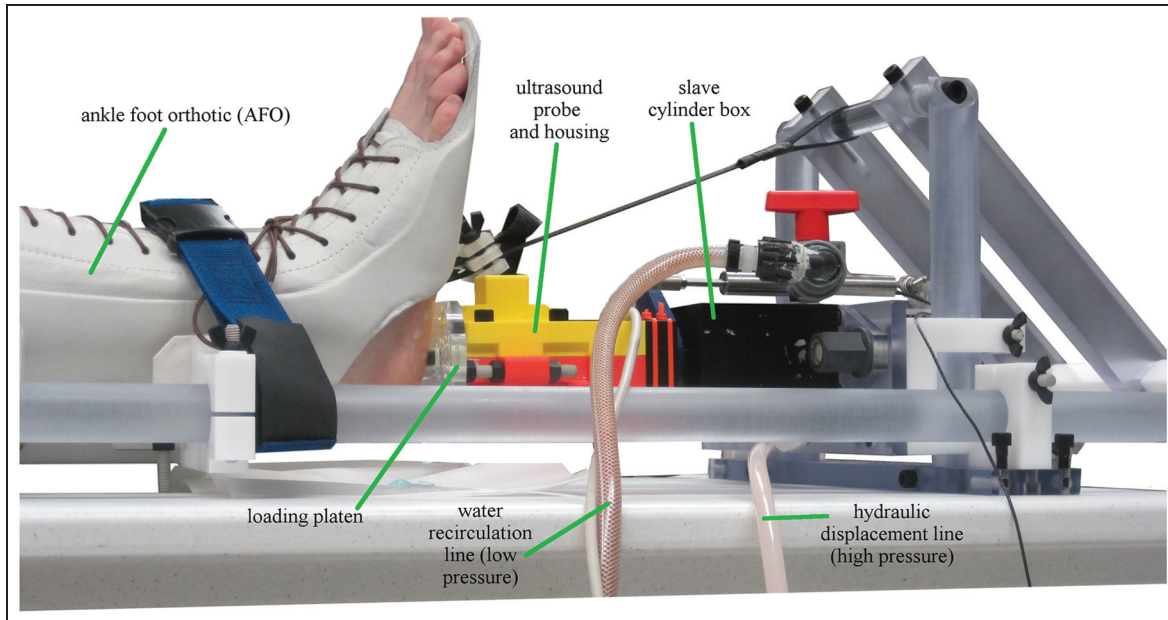


Figure 2. An ankle–foot orthosis (white) attached to polycarbonate rails secured the subject's leg and foot. The slave cylinder (black) is in series with an ultrasound probe held in ABS plastic (yellow and red) and with a polycarbonate platen. An ultrasound probe (not shown) was used to validate the system and was removed before any MRI scanning was conducted.



Figure 3. Hindfoot (white) and forefoot (black) ankle–foot orthosis. The bolts on posterior surface are for mounting to the HyPSTR loading frame.

order to capture small portions of an image volume at specific times during a loading cycle (Figure 4). These partial acquisitions from each cycle were combined to generate complete images at each phase—typically 16.

Several redundant safety measures were incorporated in the HyPSTR to protect the subject from over-loading and/or painful loading. An electronic, solenoid-operated hydraulic valve (Skinner 71295; Parker Hannifin, Cleveland, OH) was installed in the hydraulic system. When power was removed from the solenoid, the valve opened and the pressurized hydraulic fluid exited the system into a waste container, thereby removing load from the platen. Power to the solenoid could be removed by any of the following: (a) an emergency-stop button near the test operator, (b) an emergency-stop button at the test subject's side inside the MRI, (c) by the system software if a patient-specific not-to-exceed pressure was surpassed, and (d) by a virtual button on the LabVIEW front panel. The not-to-

exceed pressure was the system pressure at the subject's ground reaction force increased by a factor of 1.2 to account for pressure surges. The emergency-stop button inside the MRI was fiber-optic and interfaced with a controller (both from Banner Engineering, Minneapolis, MN) inside the MRI control room. The hydraulic system also included an adjustable mechanical pressure relief valve in case the solenoid failed. This valve was set to release any pressure greater than the patient-specific not-to-exceed pressure. As a final measure, the master piston was positioned in the master cylinder such that if it were to extend beyond a failed electronic limit switch, it could travel less than 1 mm before contacting the rigid aluminum cylinder bottom.

Verification testing

A series of verification tests were conducted to ensure the safety system and quantify the device's

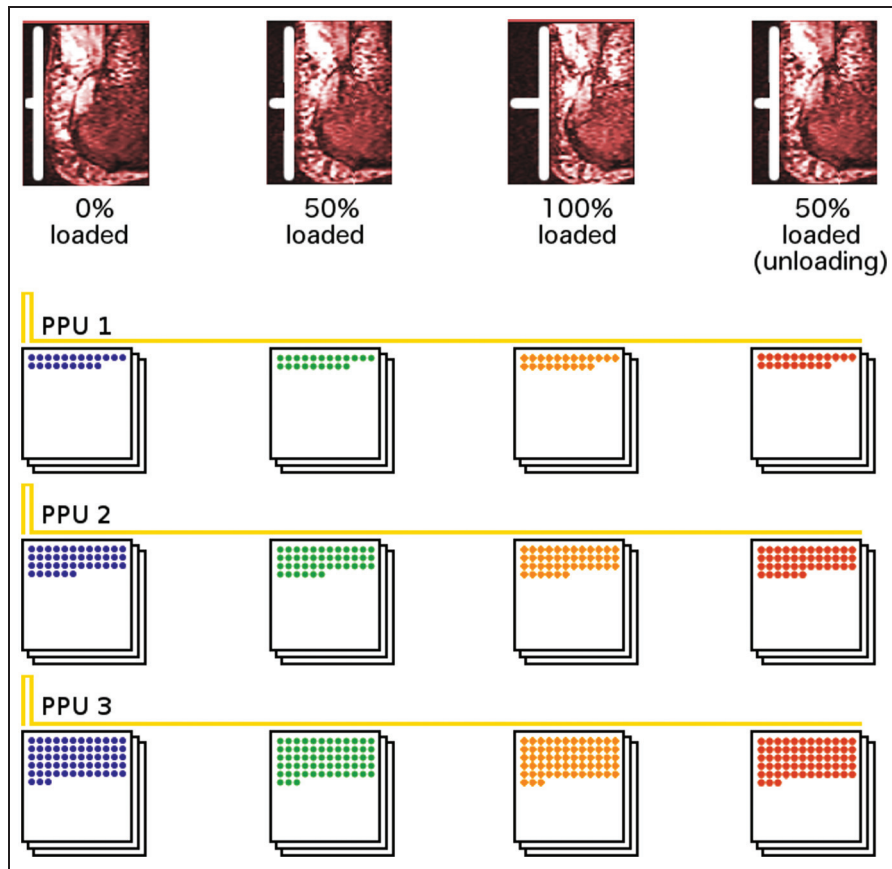


Figure 4. Gated MRI schematic showing 4 phase acquisitions for 3 cycles. The HyPSTR collected approximately 16 phases over 250 cycles during subject trials.

performance, MRI compatibility, and PPU signal generation timing. Data post-processing was performed in MATLAB (The Mathworks Inc., Natick, MA), Excel (Microsoft, Redmond, WA), and Image J (National Institute of Mental Health, Bethesda, MD).

Safety system. The hydraulic plumbing integrity was tested by loading the system against a coil spring until the maximum design pressure of 1034 kPa was attained. The system was held at that level for a period of 10 min. Each element of the safety system was then tested with these conditions to ensure operation in the most critical situation.

Device performance. The feasibility of simulating conditions similar to gait was assessed by implementing a 1-Hz triangle-wave loading pattern. The repeatability of the HyPSTR was tested by conducting three separate fill/bleed/displacement test cycles of the hydraulic system at room temperature on three separate days. For each test, the empty hydraulic system was filled with fluid and air bubbles were bled. As a gold standard, a linear variable differential transformer (LVDT) was mounted in parallel with the platen. After bleeding, the system was cycled in a 0.2-Hz sinusoid 10 times to 10 mm with no slave platen resistance to obtain

baseline performance. We expected to observe 10 mm of platen movement for every 10 mm of driving actuator movement.

A pressure step test was performed by cycling the instrument through six staircase profiles against a piece of silicone gel between the platen and a rigid backstop with the LVDT mounted in parallel with the platen. The silicone gel measured approximately 75 cm^2 with a thickness of 2 cm and was chosen due to its viscoelastic similarity to biological soft tissue. For each cycle, the actuator was advanced in 2 mm increments from 0 to 20 mm with a three-second pause following each move. After pausing at 20 mm, the actuator returned to 0 mm in one continuous motion and then the next cycle commenced ($n = 6$). This entire process was repeated three times, approximately 2 h apart, yielding a total of 18 staircase data sets. These data were used to generate a target to actual (i.e. slave to master) calibration curve for all loaded tests.

Sine-wave displacement profiles with peak platen amplitudes of 3.0, 5.0, 7.0, and 9.0 mm (as determined by the LVDT mounted in parallel with the platen) were cycled for 30 min each. The same piece of silicone gel was placed between the loading platen and the load cell. A literature review found that unloaded adult plantar soft tissue under the metatarsals and calcaneus is generally between 5.4 and 26.5 mm thick, and that the

AQ2

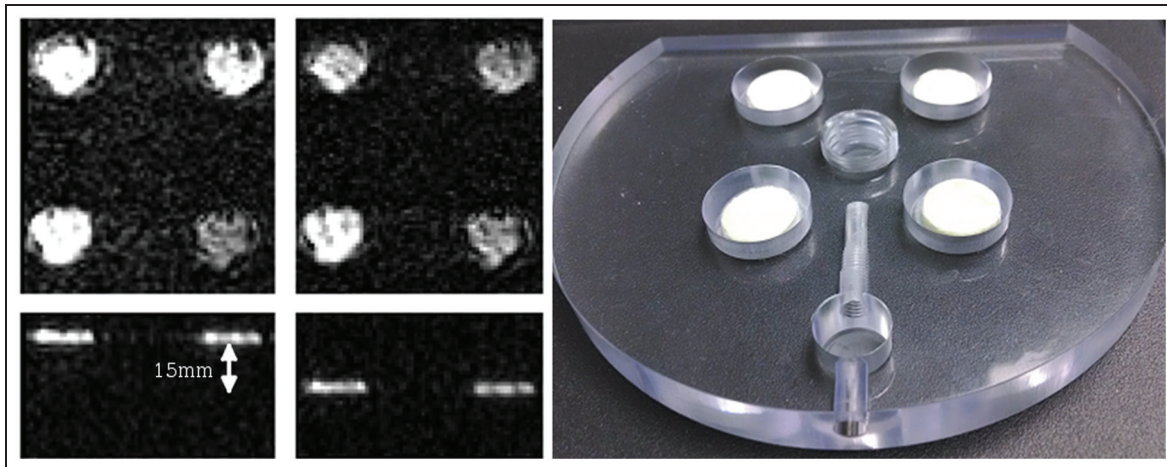


Figure 5. Platen markers from the starting position and the most extended position (15 mm travel) of a timing verification test. The platen is pictured on the right.

maximum strain in the soft tissue beneath either location under body weight is approximately 0.45.^{12–18} For each test, the actual displacement of the loading platen versus the prescribed displacement was analyzed at maximum extension for each cycle. Data from the first 10 cycles were excluded from that analysis due to preconditioning of the silicone gel. The root mean square error (RMSE) between a best-fit curve to the actual motor displacement and the prescribed displacement was calculated. Calibration curves correlating load on the platen with pressure in the system during loading and unloading were calculated for each displacement test.

MRI compatibility. The MRI compatibility of the HyPSTR was determined by quantifying the influence of the loading device upon the obtained images.²¹ A fluid-filled MRI phantom was imaged under four separate conditions: the loading device not present on the MRI table, the device in place, the device in place with electrical power on, and the device in place with electrical power on and the platen moving. This was repeated with an MRI-compatible encoder attached to the platen. A central, 2D slice of the phantom was taken from each condition and the MRI compatibility was calculated by computing the total pixel intensity delta between tests.

PPU signal generation timing. Gated MRI quality also depends on precise system synchronization. If the HyPSTR actuator motor was out of phase with the imaging protocol, then parts of the loading cycle would not be recorded and/or phases would seem out of focus, similar to motion blur. The three major sources of timing error are: (a) delays or advances in the transmission of the PPU signal to the MRI control hardware (i.e. the PPU offset), (b) discrepancy in the PPU generation period relative to the HyPSTR platen period (i.e. the

PPU phase offset), and (c) other unknown sources. The total error was determined by comparing the platen position as measured with the LVDT outside of the MRI core room to a subsequent scan with fiducial markers adhered to the platen (Figure 5).

Results

Safety system

A simple static pressure test with the coiled spring proved that the system did not have any major leaks, and high-pressure tests confirmed the proper functioning of all safety relief mechanisms. No bubbles were observed in the semi-translucent high-pressure tubing, indicating that the dissolved gas was being removed.

Device performance

Prior to testing at 6 Hz, problems with the quality of the pressure signal at 1 Hz (Figure 6(a)) were identified during the 5-mm triangle-wave tests. Because of the rapid starting and stopping of the water column, a water hammer was observed. Subsequently, 5 mm sine-wave signals with a maximum frequency of 0.2 Hz were used in order to obtain usable pressure data (Figure 6(b)).

Additional unloaded 10 mm sine-wave tests were very accurate and precise over three trials with 10 cycles each. However, there was some displacement loss: the maximum slave platen movement was 9.68 ± 0.01 , 9.65 ± 0.01 , and 9.66 ± 0.01 mm for the three separate trials. Further investigation showed that, due to machining inconsistencies, the master hydraulic piston diameter was approximately 96.5% as wide as the equivalent slave piston component. Hence, the maximum displacement for the slave piston should have been approximately 9.65 mm; all trials were within 0.03 mm or 0.31% of this value.

As load was incrementally increased against the silicone pads for the stepped pressure test, the encoder and LVDT measured a near-linear relationship between the master and slave displacements up to 8 mm (Figure 7(a) and (b)). Due to system compliance, non-linear losses occurred at the higher pressure values, where a 20-mm master displacement moved the slave

platen only 14.3 mm. For each set of six staircases, the first staircase was considered a preconditioning phase (i.e. the results were different from the other 5) and not included in displacement averaging; thus, 15 staircase profiles remained (Figure 7(b)).

Displacement and frequency accuracies were near or below 1.0% in all, but one condition for the 30-min loaded cycling tests for slave platen target positions. The displacements were least accurate in the 9-mm trial, while the frequencies deviated the most in the 3-mm trial (Table 1). Displacement precision (standard deviation divided by actual displacement) was 0.3%–1.3% and frequency precision was 0.3%–0.4% from mean values, depending on the target. (Note that these platen displacements generate the expected pressure range for subsequent in vivo testing.) The average encoder movement and the target curve used to command the encoder demonstrated good tracking with an RMSE of 0.002 mm (Figure 8). The actuator/encoder had to move 3.526 mm to make the slave platen move 3.000 mm due to system compliance, and there was a lag between the actuator and platen displacement (Figure 8). Pressure-to-force calibration curves showed different patterns for loading versus unloading (Figure 9).

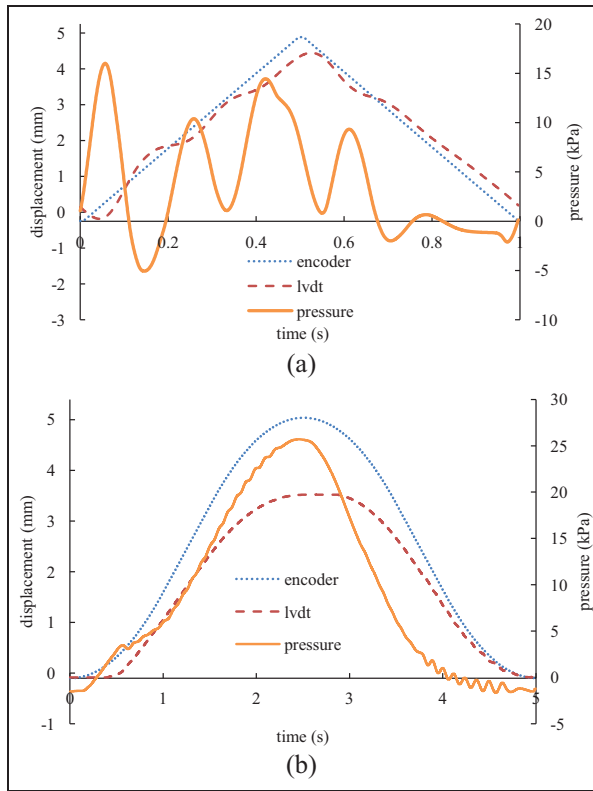


Figure 6. (a) Average of 240 triangle-wave cycles at 1 Hz and 5 mm actuator displacement and (b) average of 240 sine-wave cycles at 0.2 Hz and 5 mm actuator displacement.

MRI compatibility

MRI with a cylindrical phantom container in the acquisition volume showed no major artifacts (Figure 10(a)). For comparison, a temporary addition of two 5 virtual design and construction (VDC) copper wires to power an MRI-compatible encoder caused two parallel line artifacts to appear (Figure 10(b)). Numeric subtractions between summed image pixel intensities showed a difference of approximately 5% without the encoder and 7% with it (Table 2). Two radiologists confirmed that

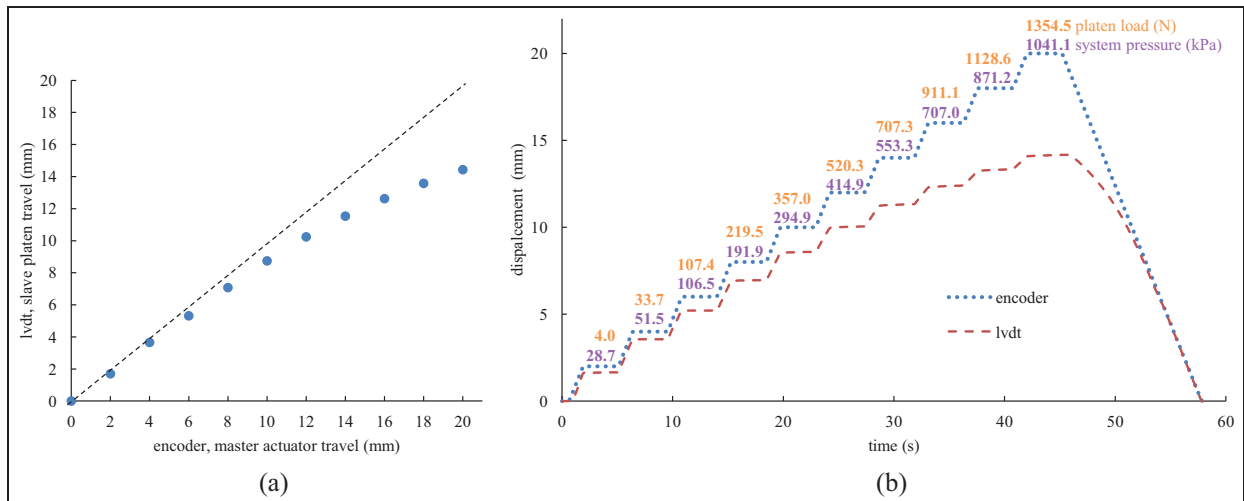


Figure 7. (a) Slave cylinder displacement versus master cylinder displacement and (b) slave platen and master cylinder displacement. The displacement loss was non-linear becoming more significant with increasing master movement. It was approximated with a polynomial and used to calculate motor parameters for future tests.

Table I. Accuracy and precision values for the HyPSTR during loading of a piece of silicon.

Target displacement (mm)	Actual displacement (mm)	Error (%)	Target frequency (Hz)	Actual frequency (Hz)	Error (%)	Pressure (kPa)
3.000	3.05 ± 0.04	1.67	0.1775	0.1780 ± 0.0008	0.28	48.7
5.000	4.99 ± 0.06	0.20	0.1814	0.1816 ± 0.0006	0.11	104.1
7.000	7.074 ± 0.02	1.06	0.1794	0.1796 ± 0.0006	0.11	203.5
9.000	9.373 ± 0.08	4.14	0.1782	0.1785 ± 0.0005	0.17	351.8

All data were from a linear variable differential transformer attached to the slave platen.

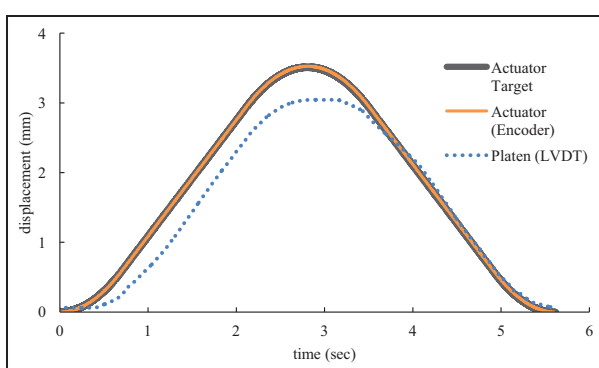


Figure 8. Overlap of the target sine wave used to set the motor control parameters and resulting encoder movement. The encoder path is nearly identical to the prescribed curve (shown with an exaggerated thickness).

early.²² This means that there is still a 31.5- to 33.5-ms advance offset that we are unable to locate.

Discussion

Foot anatomy and material properties are unique to each individual and dependent on loading rates. If the tools used to assess foot mechanics (e.g. FEA models) are able to account for these subject-specific differences, especially for populations with abnormally stiff plantar soft tissue such as persons with diabetes, this could lead to better treatment options. MRI is capable of providing the necessary image quality and tissue differentiation for these foot model improvements, but requires a compatible loading device. The functionality of the HyPSTR demonstrates progress toward a non-metallic, hydraulic system with repeatable performance to physiologic loading levels.

Device performance

The maximum achievable cyclic rate was 0.2 Hz because of the erratic pressure signals at higher frequencies. This was caused by a “water hammer,” which is a series of pressure reflections when attempting to rapidly reverse the momentum of the water column inside the hydraulic tubing (Figure 6(a)). The high frequency oscillations to the left of the maximum and minimum peaks were likely from the piston not being able to move smoothly past its friction point at slower velocities (Figure 6(b)). A pressure snubber could potentially be used to attenuate this ringing. Other possible solutions are to reduce the high-pressure tubing diameter to lower the mass of the water column or use a more compressible, viscous hydraulic fluid, such as glycol or oil, which can dampen the surges. The tradeoff for all of these changes is lower platen force per unit of pressure, but it is still worth considering because the plantar fat pad modulus has been shown to change significantly between 1 and 10 Hz loading in cadaveric samples.²

The frequencies of the vertical ground reaction force of human gait would be more accurately simulated by impact loading profiles instead of sine waves. While virtually any motion profile may be programmed into the HyPSTR, it is currently limited to sinusoidal patterns that give cleaner pressure signals than a more appropriate (multi-frequency) triangle wave. Ultrasound

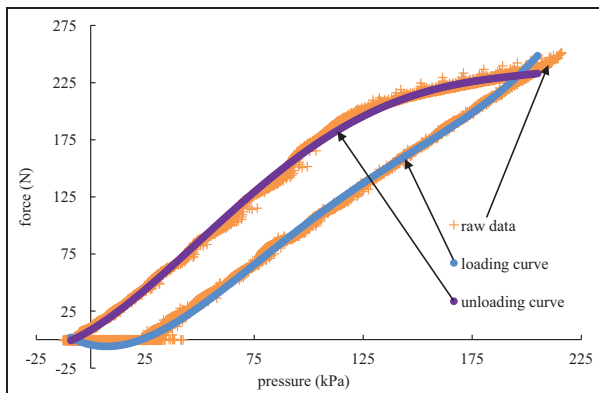


Figure 9. Pressure to force calibration curve from the 7-mm loaded verification test.

the pixel quality observations did not indicate any significant artifacts.

PPU signal generation timing

The two timing verification tests showed that the platen position data from the MRI was collected 5.48 and 7.38 ms earlier than in the LVDT test. These values show a smaller than expected error; based on the measurable PPU offset and PPU phase offset, we expected the MRI data to be acquired approximately 39 ms

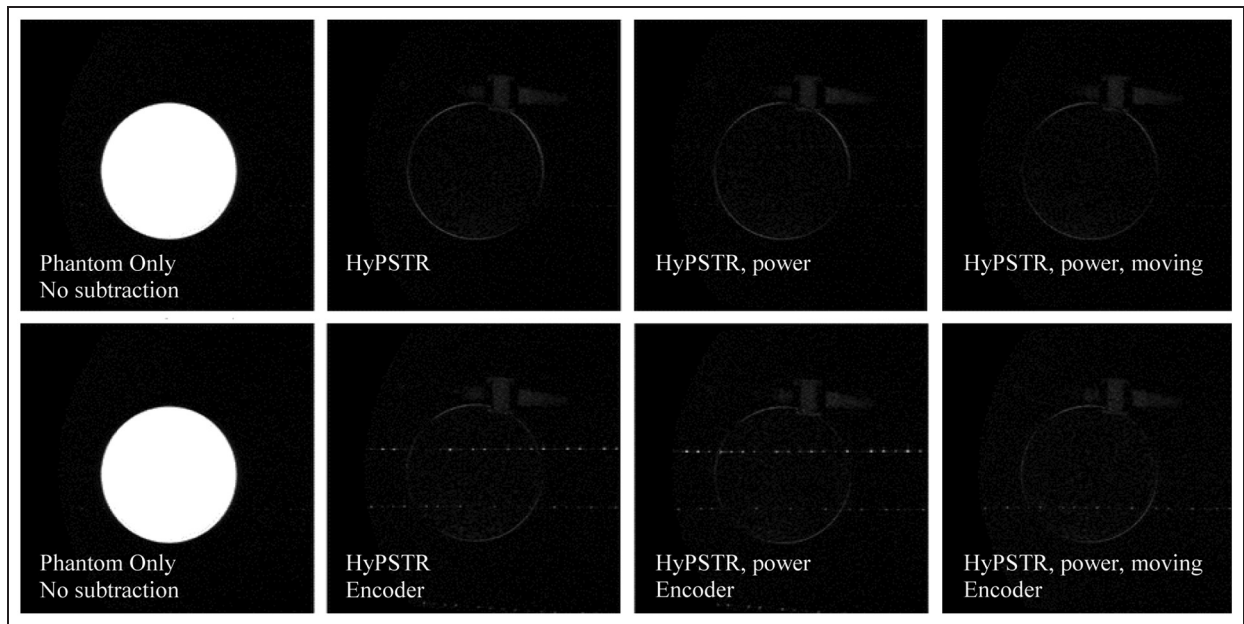


Figure 10. The leftmost images are of the control phantom without any hardware in the MR core. The darker images are subtractions of the same phantom, but with different system configurations. (a) Top row is without the encoder and (b) bottom row is with the encoder. Second column is only hardware; third column is hardware plus power; and fourth column is hardware, plus power and plus actuator motion.

AQ3

Table 2. Quantitative artifact analysis.

Test condition	Pixel intensity (normalized)	Relative intensity to phantom only (%)
Phantom only (no image subtraction)	1,111,615	100.0
HyPSTR	58,526	5.1
HyPSTR, powered	60,971	5.5
HyPSTR, powered, moving	60,320	5.4
HyPSTR with encoder	73,912	6.6
HyPSTR with encoder , powered	76,031	6.8
HyPSTR with encoder , powered, moving	81,300	7.3

The tests with the MRI-compatible encoder increased artifact pixel intensity compared to those without the encoder..

AQ4

instruments that permit true subject motion on a walking platform have a great advantage in this regard,⁶ but the studies to date have generated two-dimensional data and are subject to trial-to-trial variability.

The HyPSTR produces accurate and precise movement for both unloaded and loaded platen conditions (Table 1). Though there was some system compliance (Figure 7(a)), the hydraulics can apply enough force to equal the body weight of 138 kg (1354.5 N) subject (Figure 7(b)). Forces near this magnitude have been achieved before with MRI-compatible devices,⁸ but not in conjunction with dynamic loading. The LVDT displacement magnitude lagged behind the encoder because of the time required for the system to build up the approximately 30 kPa of pressure that was needed to overcome static friction in the slave cylinder (Figure 8). The effect of the static friction can be seen on the bottommost and topmost parts of the loading curve (i.e. hysteresis), where changes in pressure did not immediately affect the applied force (Figure 9).

MRI compatibility

Pixel comparisons of a phantom object in the MR core during various configurations of equipment, power state, and movement show that there is little concern for artifact contamination in future foot data sets (Table 2). The noncircular, gray shapes in the background were thought to be areas of water in the plumbing fittings and are located outside of the foot image volume. An obvious problem was caused by a copper wire leading to a platen encoder; the encoder was removed to be certain that we recorded the highest image quality. Though the encoder artifacts probably would not have affected the ability to measure mechanical properties (i.e. 7.3% is relatively similar to 5.4% added pixel brightness), there were additional issues with providing enough voltage to the sensor head over a 9-m long small gauge wire. A fiber-optic potentiometer might have been a better choice,²³ but commercial options were limited. Instead, the four inset MRI

fiduciary markers provided a means of tracking the platen by generating a best-fit plane parallel to the foot contact surface.

PPU signal generation timing

There was an unknown timing error between the MR image acquisition and device actuator movement of 32.5 ms that has been empirically verified. This error might be due to the serial to fiber-optic PPU conversion that is required to read the PPU signal into the MRI scanner. Additionally, once the PPU signal is received by the MRI scanner, there could be an internal delay within the system.

Future work and conclusion

Future work will focus on exploring different hydraulic fluids, installing a double acting hydraulic piston, considering fiber-optic encoders, and precisely determining gated MRI timing. These efforts will address the limitations regarding the water hammer, pressure-force hysteresis, MRI displacement tracking, and HyPSTR-to-MRI synchronization. We will also use the HyPSTR to test forefoot tissue properties. The device and methods from this work will be used to collect *in vivo* data for inputs and benchmarks for patient-specific FEA foot models under development.

The HyPSTR aims to compliment the capabilities of MRI technology in order to determine patient-specific material properties. It allows for non-invasive, internal measurements of the foot's plantar soft tissue in dynamic loading conditions. With this information and FEA modeling techniques, it may be possible to locate and quantify high stress regions within the foot that can help explain the cause and prevention of structural tissue damage.

Acknowledgements

John Shaffer helped with design consultation and construction of the ankle-foot orthotics at American Artificial Limb, Seattle, WA.

Declaration of conflicting interests

The author(s) declared no potential conflicts of interest with respect to the research, authorship, and/or publication of this article.

Funding

This work was supported by the Department of Veterans Affairs, Rehabilitation Research & Development Service grant A6973R.

References

1. Centers for Disease Control and Prevention. *National diabetes fact sheet, 2014*. Atlanta, GA: Centers for Disease Control and Prevention, 2014.
2. Pai S and Ledoux WR. The compressive mechanical properties of diabetic and non-diabetic plantar soft tissue. *J Biomech* 2010; 43: 1754–1760.
3. Gefen A. Plantar soft tissue loading under the medial metatarsals in the standing diabetic foot. *Med Eng Phys* 2003; 25: 491–499.
4. Bakker K, Apelqvist J and Schaper NC. International Working Group on Diabetic Foot Editorial B. Practical guidelines on the management and prevention of the diabetic foot 2011. *Diabetes Metab Res Rev* 2012; 28(Suppl. 1): 225–231.
5. Gefen A, Megido-Ravid M and Itzchak Y. In vivo biomechanical behavior of the human heel pad during the stance phase of gait. *J Biomech* 2001; 34: 1661–1665.
6. Cavanagh PR. Plantar soft tissue thickness during ground contact in walking. *J Biomech* 1999; 32: 623–628.
7. Erdemir A, Viveiros ML, Ulbrecht JS, et al. An inverse finite-element model of heel-pad indentation. *J Biomech* 2006; 39: 1279–1286.
8. Petre M, Erdemir A and Cavanagh PR. An MRI-compatible foot-loading device for assessment of internal tissue deformation. *J Biomech* 2008; 41: 470–474.
9. Gefen A, Megido-Ravid M, Azariah M, et al. Integration of plantar soft tissue stiffness measurements in routine MRI of the diabetic foot. *Clin Biomech* 2001; 16: 921–925.
10. Brown PJ, Tan H and Stitzel JD. Displacement control device for dynamic tissue deformation in MRI—biomed 2010. *Biomed Sci Instrum* 2010; 46: 99–104.
11. Weaver JB, Dooley M, Cheung Y, et al. Imaging the shear modulus of the heel fat pads. *Clin Biomech* 2005; 20: 312–319.
12. Fields ML, Greenberg BH and Burkett LL. Roentgenographic measurement of skin and heel-pad thickness in the diagnosis of acromegaly. *Am J Med Sci* 1967; 254: 528–533.
13. Gooding GA, Stess RM, Graf PM, et al. Sonography of the sole of the foot. Evidence for loss of foot pad thickness in diabetes and its relationship to ulceration of the foot. *Invest Radiol* 1986; 21: 45–48.
14. Kanatli U, Yetkin H, Simsek A, et al. The relationship of the heel pad compressibility and plantar pressure distribution. *Foot Ankle Int* 2001; 22: 662–665.
15. Kwan RL, Zheng YP and Cheung GL. The effect of aging on the biomechanical properties of plantar soft tissues. *Clin Biomech* 2010; 25: 601–605.
16. Prichasuk S. The heel pad in plantar heel pain. *J Bone Joint Surg Br* 1994; 76: 140–142.
17. Prichasuk S, Mulpruek P and Siriwongpairat P. The heel-pad compressibility. *Clin Orthop Relat Res* 1994; 300: 197–200.
18. Uzel M, Cetinus E, Ekerbicer HC, et al. Heel pad thickness and athletic activity in healthy young adults: a sonographic study. *J Clin Ultrasound* 2006; 34: 231–236.
19. Antonsson EK and Mann RW. The frequency content of gait. *J Biomech* 1985; 18: 39–47.
20. Van de Walle R, Lemahieu I and Achten E. Magnetic resonance imaging and the reduction of motion artifacts: review of the principles. *Technol Health Care* 1997; 5: 419–435.
21. Tsekos NV, Khanicheh A, Christoforou E, et al. Magnetic resonance-compatible robotic and mechatronics systems for image-guided interventions and rehabilitation: a review study. *Annu Rev Biomed Eng* 2007; 9: 351–387.

22. Williams ED. *Hydraulic plantar soft tissue reducer—structural properties of the human heel pad*. Washington, DC: Mechanical Engineering Department, University of Washington, 2015.
23. Belforte G and Eula G. Design of an active-passive device for human ankle movement during functional magnetic resonance imaging analysis. *Proc IMechE, Part H: J Engineering in Medicine* 2011; 226: 21–32.
24. Isvalinonda V. *Finite element modeling of the foot*. Washington, DC: Mechanical Engineering Department, University of Washington, 2015.

AQ5